Enhanced post-fault recovery in MTDC networks using active damping approach

Sharma, Monika; Torres, José L.Rueda

DOI
10.1049/gtd2.13321

Publication date
2025

Document Version
Final published version

Published in
IET Generation, Transmission and Distribution

Received: 9 August 2024 | Revised: 16 October 2024 | Accepted: 30 October 2024

IET Generation, Transmission & Distribution

DOI: 10.1049/gtd2.13321

The Institution of Engineering and Technology WILEY

ORIGINAL RESEARCH

Enhanced post-fault recovery in MTDC networks using active damping approach

Monika Sharma | **José L. Rueda Torres**

Department of Electrical Sustainable Energy, TU Delft, Delft, Netherlands

Correspondence
Monika Sharma and José L. Rueda Torres, Department of Electrical Sustainable Energy, TU Delft, Delft, Netherlands.
Email: sharmamonika.6636@gmail.com and j.l.ruedatorres@tudelft.nl

Funding information
European Union's Horizon Europe, Grant/Award Number: 101075424; UK Research and Innovation, Grant/Award Numbers: 10041877, 10051113

Abstract

The increasing deployment of offshore wind farms necessitates robust and stable high-voltage direct current networks. Achieving optimal stability, especially in damping oscillations on the DC side, remains a significant challenge. This study focuses on mitigating post-fault converter de-blocking oscillations, a critical issue exacerbated by complex interactions between AC and DC systems, converter dynamics, and system faults. These behavior are governed by nonlinear system dynamics, making traditional control methods less effective in ensuring stability. A comprehensive analysis of DC side oscillations and their interaction with converter dynamics is developed to understand the key factors influencing system stability. The research investigates a DC voltage regulation damping approach, identified as the most effective solution in the literature. Comprehensive parametric sensitivity analysis evaluates system behavior under diverse operational conditions. Addressing current damping method limitations during converter de-blocking, this work proposes an innovative control approach integrating fuzzy logic control and proportional–integral controllers. This approach enhances DC voltage regulation and incorporates a modified circulating current suppression control in the inner loop. The coordinated fuzzy logic control and proportional–integral controller dynamically adjusts to nonlinear system dynamics in real-time, providing a robust framework for improved post-fault recovery. It aims to achieve faster recovery times and reduced overshoot compared to conventional methods. The proposed controller's efficacy is validated through comparative analysis with existing approaches. Electromagnetic transient) simulations using the real-time digital simulator platform demonstrate the controller's performance under realistic operating conditions.

1 | INTRODUCTION

The burgeoning growth of offshore wind farms necessitates robust and efficient power transmission solutions. High-voltage direct current (HVDC) transmission based on voltage-sourced converter (VSC) technology is rapidly emerging as a leading contender for this task [1]. Several studies have shown that VSC-HVDC offers distinct advantages over traditional AC transmission for long-distance applications, particularly those involving offshore wind farms [2]. Firstly, unlike AC transmission which suffers from power limitations due to cable capacitance, VSC-HVDC systems are not constrained by distance. This makes them ideal for connecting offshore wind farms located far from shore to mainland networks. Secondly, VSC-HVDC offers superior controllability compared to AC transmission. This enables valuable features like power oscillation damping (POD) to mitigate inter-area oscillations within the AC system. Additionally, VSC-HVDC facilitates the operation of multi-terminal HVDC networks (VSC-MTDC), paving the way for interconnected offshore networks across national borders [1, 2].

As VSC technology evolves from low voltage and capacity to high voltage and capacity, the modular multi-level converter (MMC) is becoming the mainstream method for constructing HVDC networks [3]. MMCs offer several advantages over traditional two-level VSC systems. Firstly, the output voltage at the

AC terminal can be close to an ideal sinusoidal waveform, eliminating the need for filters at the point of common coupling (PCC) [4]. Secondly, the expansion of DC voltage and capacity can be easily achieved by increasing the number of sub-modules in each arm, making MMCs a scalable solution for HVDC transmission systems [3]. This development in VSC technology paves the way for larger and more complex HVDC networks.

While HVDC offers numerous benefits for integrating offshore wind farms, its integration into existing power networks presents new challenges regarding oscillation control and system stability [5]. The presence of significant inductance and stray capacitance in long HVDC cables can introduce poorly damped oscillations that interact with the control systems of power electronic converters, potentially leading to over-voltages and even system instability [6]. These oscillations at the DC side are particularly concerning, as current peak overshoots and large settling times can interact with converter control loops and lead to grid failures or blackouts. To theoretically explain the occurrence of these oscillations, the mathematical model is discussed in [7] with DC side equivalent circuit of the converter with non-linear dynamics and internal parameters (e.g. capacitance and inductance). These factors contribute to resonance and poor damping behaviour. Post-fault oscillations during deblocking of converter have been widely observed and are exacerbated by non-optimally tuned controllers and current limitations. These oscillations are particularly critical when the inverter is connected to weak grids, necessitating the use of adaptive damping techniques such as virtual resistors or flexible control schemes to stabilize voltage and frequency during fault recovery periods [8, 9].

Various supplemental controllers have been proposed to enhance damping on the DC side of HVDC networks. For example, Liu et al. implemented D-Q circulating current suppression control (CCSC) with modulated signals, achieving a 2.59% reduction in overshoot and a 3.57% reduction in settling time compared to conventional methods [10]. Virulkar et al. integrated CCSC with model predictive control (MPC), resulting in a 13.6% reduction in settling time compared to traditional PI control [11]. Li et al. introduced a novel virtual active damping or resonance suppression strategy to maintain DC-link voltages within acceptable limits [10, 12]. Additionally, Wu et al. explored virtual synchronous generators using virtual inertia and damping control with a proportional-derivative controller to enhance DC network stability [13]. Despite these advancements, traditional damping methods like impedance-based and active damping control often require additional hardware or face parameter tuning challenges [14, 15].

A critical knowledge gap exists regarding damping control in meshed HVDC networks compared to point-to-point (P2P) configurations. Existing research predominantly focuses on P2P systems, neglecting the intricate dynamics present in meshed networks due to their complex topologies and potential for multi-modal interactions. This necessitates further investigation into control strategies specifically designed for meshed networks [16, 17]. Additionally, current damping control methods might not fully address the non-linearities that arise during converter de-blocking [18–20]. These non-linearities can introduce transient behaviours that may not be adequately captured by existing control algorithms. Consequently, the limited ability to handle non-linearities can lead to insufficient damping and potentially contribute to instabilities on the DC side. Addressing these limitations and exploring control strategies for meshed networks with converter de-blocking considerations is crucial for ensuring stable and reliable HVDC network operation.

Traditional PI controllers are widely used for damping control due to their simplicity and effectiveness in linear systems. However, HVDC systems can exhibit non-linear behaviour under certain conditions (e.g. short circuit faults), limiting the performance of PI controllers. These nonlinearities stem from the interactions between converter switching dynamics and cable capacitance, causing sudden changes in system stability margins. Traditional PI controllers, which are based on linear control theory, struggle to address these transient phenomena effectively.

Modern control techniques, such as fuzzy logic control (FLC), offer promising alternatives for non-linear systems [21, 22]. FLC is particularly effective when system information is lacking or complexity impedes comprehensive analysis, as it can handle imprecise or incomplete data. Fuzzy set theory, pioneered by Lotfi Zadeh, applies to control functionalities, especially for damping oscillations in HVDC networks, by incorporating system behavior ambiguity into the control strategy [23]. FLC requires fewer computational resources compared to other intelligent control techniques, making it more efficient for real-time applications [24].

This research investigates a novel damping control method to improve post-fault (PF) recovery in HVDC networks. The proposed method employs an enhanced DC voltage regulation control mechanism in the outer control loop with modified CCSC in the inner control loop. This study proposes a coordinated FLC and PI controller for improved damping performance. The mathematical foundation of the proposed controller is based on nonlinear control theory, where FLC compensates for uncertainties, and PI ensures stable operation under nominal conditions. The FLC adapts the control strategy in real-time to handle non-linearities, while the PI controller provides a robust framework for overall system performance, potentially leading to faster settling times and reduced overshoot compared to traditional methods.

The main contributions of this article are summarized as follows:

1. **Identification of the optimal damping approach**: This work analyzes various damping techniques for the DC side of HVDC networks. It identifies a combination of DC voltage regulation control in the outer loop and an enhanced current control loop for MTDC networks as the most effective approach. Additionally, a comprehensive parametric sensitivity analysis is conducted to evaluate the system's performance under different conditions [7].
2. **Proposed fuzzy-PI controller for improved post-fault recovery**: The article introduces a novel controller that addresses non-linearities in the system to enhance post-fault recovery. This fuzzy-PI controller is compared with existing controllers from the literature to demonstrate its effectiveness.

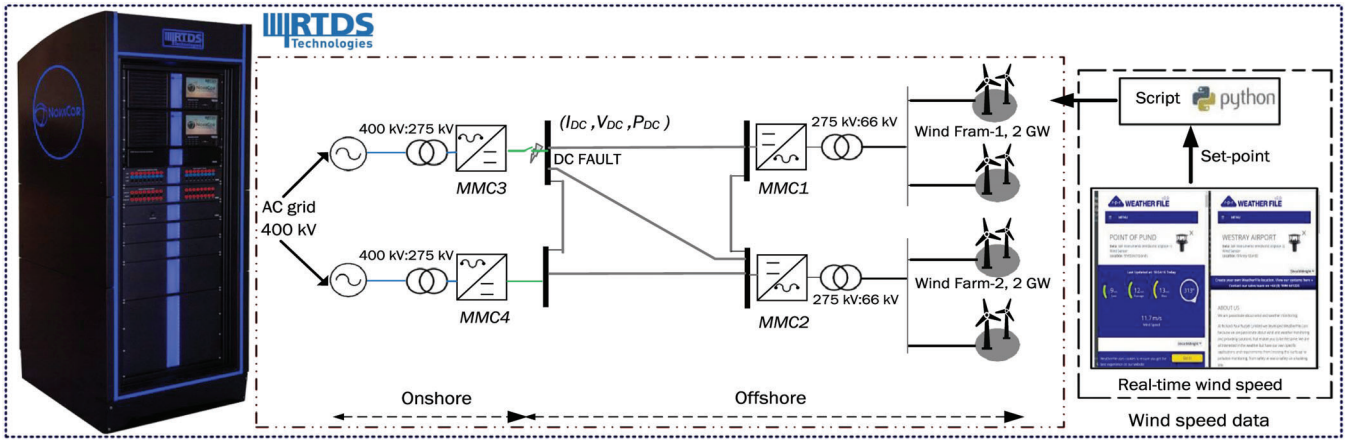

FIGURE 1 A four-terminal ±525 kV half-bridge MMC-based MTDC network.

The remainder of this paper is organized as follows. Section 2 elaborates on the system model. Sections 3 and 4 cover the system stability mechanisms in MTDC networks, along with an analysis of the active damping controller and the enhanced CCSC. Sections 5 and 6 describe the approach used for parametric sensitivity analysis and the results obtained after fine-tuning the key parameters. Section 7 presents the proposed controller and offers a comprehensive analysis of the results obtained. In Section 8, the work is concluded.

2 | SYSTEM MODEL

A four-terminal MMC-based MTDC network with a DC voltage rating of ±525 kV and a bipolar dedicated metallic return (DMR) configuration is considered for this study, as shown in Figure 1. The converter uses a half-bridge topology. The system can be divided into two subsystems: the onshore system and the offshore system. The rated line-to-line (LL) voltage is 400 kV. The onshore converter station has two Y-D transformers, each with a rating of 2 GVA. The voltage ratio of these transformers is 400 kV/275 kV. The onshore converters are labelled MMC3 and MMC4.

For the four-terminal HVDC network, the length of the onshore cables is 12 km up to the PCC, as indicated by the green-coloured onshore DC cable. The land cables connect the onshore DC hub, which comprises DC switch. For simplicity and to reduce the computation burden, only one DC switch is employed. Furthermore, the DC system comprises five subsea cable links (300 km length of all the subsea cables). The cables are modelled as frequency phase-depended model. Furthermore, the cable link consists of three conductors (i.e. a positive, a negative cable, and metallic return per cable link) due to DMR topology [1].

The offshore AC system consists of converter stations and aggregated average-value model wind farms. In the applied networks, offshore converters are labelled MMC1 and MMC2. The offshore converter is connected to the offshore AC system via D-Y transformers. The rating of this transformer is 275 kV/220 kV, 2 GVA. Besides, this converter transformer is connected to a wind turbine transformer. This transformer has a voltage ratio of 220 kV/66 kV and acts as a VA scaled-up transformer.

TABLE 1 Converter station parameters [25].

Parameters	Onshore converter station per MMC	Offshore converter station per MMC
Rated power	2000 MVA	2000 MVA
Fundamental frequency	50 Hz	50 Hz
AC grid voltage	400 kV	220 kV
AC converter bus voltage	275 kV	275 kV
Bus voltage		
DC link voltage	525 kV	525 kV
Number of submodules per valve	240	200
Rated voltage and Current of each Submodule (SM)	2.5 kV/2 kA	2.5 kV/2 kA

Table 1 lists the converter station parameters with associated values used in this work. The wind turbine model used for this study is a Type 4 model [4]. It has a rating of 2 MW at a wind speed of 15 m/s.

The wind speed data is uploaded to RSCAD/RTDS via co-simulation as depicted in Figure 1. The TCP/IP protocol connects RSCAD/RTDS to the Python script. In this script, live wind data is collected every second from two locations (i.e. Orkney and Shetland regions) in the north sea via a website and then communicated to the wind speed slider in RSCAD/RTDS via TCP/IP protocol.

3 | SYSTEM STABILITY MECHANISM IN MMC-BASED MTDC NETWORK

The stability of an MMC-based MTDC network is fundamentally dependent on several key mechanisms, which work in tandem to ensure the reliable operation of the system. One

of the primary stability considerations is the regulation of DC voltage across the network. Voltage imbalances between the grid-side and converter DC-side can lead to disruptions in power flow, oscillations, and potentially destabilize the system. To address this, the control systems aim to maintain a stable DC voltage, particularly during transient conditions like faults or converter deblocking. In the MMC converters, which employ a half-bridge topology, the stability is also heavily influenced by the behavior of sub-modules. By dynamically adjusting the number of active sub-modules within each converter, the system can fine-tune the DC voltage, effectively preventing instability and ensuring smooth transitions during critical events.

Another important factor contributing to system stability is the interaction between the onshore and offshore subsystems. These two systems are interconnected and must balance differing AC grid voltages and subsea cable characteristics. In this context, the dedicated metallic return (DMR) topology plays a crucial role by providing a reliable return path, which helps mitigate potential oscillations and ensures stable power transfer between onshore and offshore converter stations. Furthermore, the subsea cables in this network are modeled as frequency-dependent to capture their real-world behavior accurately under varying operational conditions. This detailed cable modeling allows the system to better handle the variations in cable capacitance and inductance, which can influence stability, particularly during high-frequency oscillations.

With these mechanisms in place to ensure a stable baseline operation, the system can effectively manage disturbances and transitions, creating a strong foundation for evaluating the performance of advanced control strategies like the active damping controller and the enhanced CCSC, particularly in improving post-fault recovery.

4 | PERFORMANCE OF ACTIVE DAMPING CONTROLLER AND ENHANCED CCSC

The necessity for an active damping approach is critical for enhancing post-fault recovery in MMC-MTDC networks. This study highlights the importance of DC voltage regulation techniques, particularly when combined with the enhanced D-Q type CCSC controller. This combination shows promise in using modulated signals with CCSC to improve oscillation damping, thereby enhancing stability and performance in HVDC networks, as discussed in Section 1. The study employs parametric sensitivity analysis as a crucial means for system assessment.

4.1 | DC-voltage regulation method

The primary focus of this study revolves around the control loop of the DC voltage regulation method, as illustrated in Figure 2. Instances where the post-fault DC-side voltage consistently drops below the designated minimum threshold ($V_{\mathrm{DC}}^{\mathrm{min}}$) often lead to a disparity between the grid-side and converter DC-side voltage, attributable to the constraints of existing controls and voltage evaluation criteria. To rectify this discrepancy during the deblocking process, it becomes imperative to align the converter DC-side output voltage precisely with the grid-side voltage. This alignment is achieved by reducing the number of actively engaged sub-modules during the de-blocking moment, thereby effectively decreasing the converter DC-side voltage to closely match the grid-side voltage.

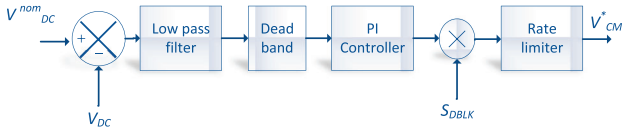

FIGURE 2 Control loop for standard DC-voltage regulation in MMC-HVDC network.

This section explores a novel control loop for DC voltage regulation during the converter deblocking process, as illustrated in Figure 2, aimed at damping the oscillations that occur during converter deblocking. Following a fault event, the DC-side voltage might consistently fall below a predefined minimum threshold ($V_{\mathrm{DC}}^{\mathrm{min}}$). This discrepancy between the grid-side and converter DC-side voltage can arise due to limitations in existing controls and voltage evaluation criteria.

To address this issue during deblocking, the proposed method aims to precisely match the converter's DC-side voltage output with the grid-side voltage. This alignment is achieved by dynamically adjusting the number of active sub-modules within the converter. By strategically reducing the number of active sub-modules during deblocking, the converter's DC-side voltage effectively decreases, minimizing the voltage difference with the grid.

The control loop operates by subtracting the control loop output from the internal voltage reference. This subtraction effectively reduces the number of active sub-modules. The controller activation is specifically triggered only during deblocking events through a dedicated signal S_{DBLK}.

A rate limiter is implemented to manage the speed at which sub-modules are adjusted. This limiter ensures a smooth transition by accelerating sub-module reduction until the nominal DC-side voltage is reached. It prevents sudden voltage fluctuations while regulating the rate of sub-module re-insertion back into operation. The difference between the nominal DC voltage and the grid voltage, referred to as the voltage error, is integrated into the controller ($G(s)$) to optimize the system response during deblocking. The integrator helps fine-tune the system's response by accounting for any persistent voltage differences.

A proportional controller is usually sufficient for regulating the DC-side voltage, often supplemented with a low-pass filter to remove unwanted high-frequency components. During normal operations, the controller output remains at zero because the DC-side voltage is near the nominal value due to the dead-band block. However, if the DC-side voltage drops below $V_{\mathrm{DC}}^{\mathrm{min}}$ at the moment of deblocking, causing the error to exceed the dead-band threshold, the controller output activates

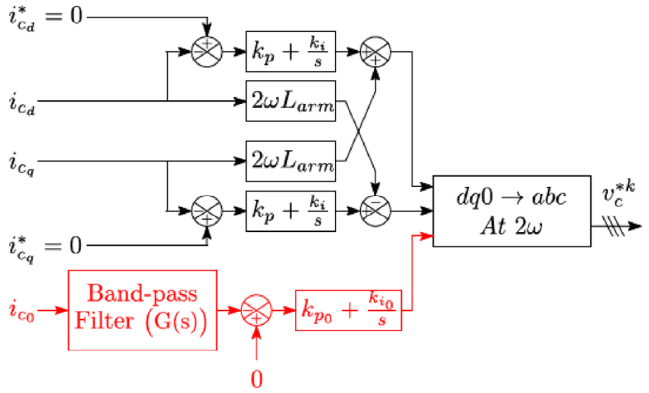

FIGURE 3 Modified D-Q CCSC [7].

to reduce the number of inserted sub-modules, thereby aligning the system with the grid voltage [7].

4.2 | Role of enhanced D-Q CCSC

As highlighted in Section 1, the utilization of the D-Q type CCSC configuration with damping controller improves damping properties while maintaining the steady-state DC current. This study involves a parametric sensitivity analysis of the enhanced D-Q type CCSC, illustrated in Figure 3. The CCSC configuration is designed to minimize the impact of zero-sequence non-DC elements in the circulating current, ensuring minimal disruption to the steady-state DC component [7].

Non-DC components infiltrate the zero-sequence component (i_{c_0}) during post-fault recovery, which ideally should only contain a DC component during steady-state operation, as depicted in Figure 3. To handle these non-DC components within the zero-sequence current, a band-pass filter is used to effectively isolate them from the DC component. Additionally, a PI controller is employed to drive these non-DC components toward zero. The band-pass filter's bandwidth is carefully chosen to cover a wide range of resonant frequencies, identified through a comprehensive analysis of DC-side resonance.

This study emphasizes the importance of carefully selecting appropriate parameters for DC voltage regulation methods and enhanced CCSC to enhance the damping of post-fault oscillations during the deblocking of the converter. The subsequent section will delve into the approach for parametric sensitivity and key parameters that need to be considered to improve post-fault recovery on the DC side of networks.

5 | APPROACH FOR PARAMETRIC SENSITIVITY

Figure 4 illustrates the proposed approach for sensitivity analysis. The process commences with the preparation of the overall dynamic model. Initially, control parameters are configured using an RTDS script. Subsequently, an EMT simulation is conducted with the initial settings to pinpoint areas for

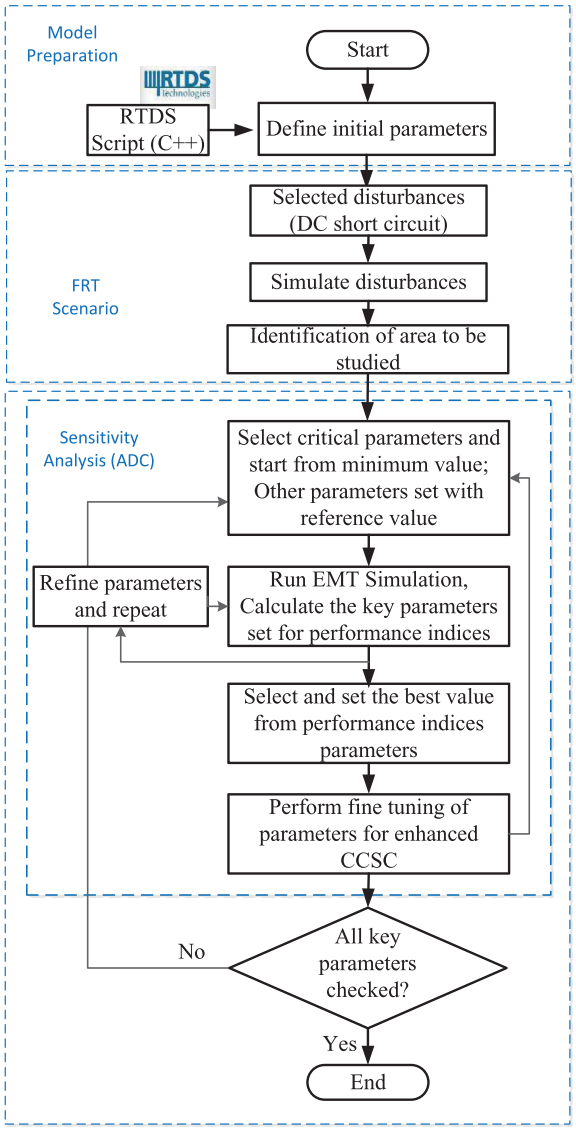

FIGURE 4 Procedure for sensitivity analysis.

improvement. This study specifically addresses a FRT scenario pertaining to the blocking of converters when a severe fault (such as a DC short circuit) occurs near the converter terminal. The effectiveness of the post-fault recovery process hinges on whether any converters in the HVDC network are in a blocked state due to the fault. Converter blocking implies that they are no longer capable of controlling their active powers in post-fault conditions. To mitigate the impact of these disturbances, the blocked converter must be promptly deblocked and actively controlled. The potential occurrence of poorly damped oscillations during post-fault recovery can be observed in current and voltage waveforms. The focus of the flowchart is on analysing the active damping controller (ADC) to improve post-fault recovery during deblocking, involving key parameter adjustments and evaluations until a satisfactory outcome is achieved to enhance the post-fault recovery of the HVDC network. Parameters are fine-tuned to ascertain the optimal set point from a wide range of values. A similar analysis is conducted for the enhanced

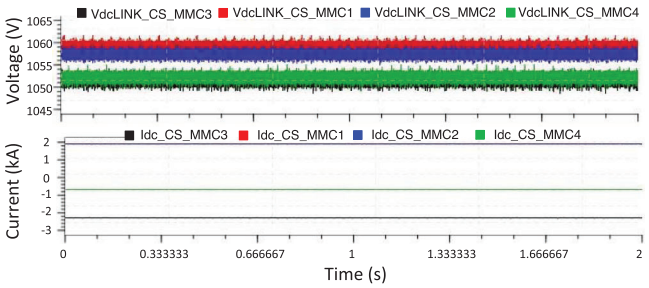

FIGURE 5 Initial currents and voltages at DC side of MTDC network.

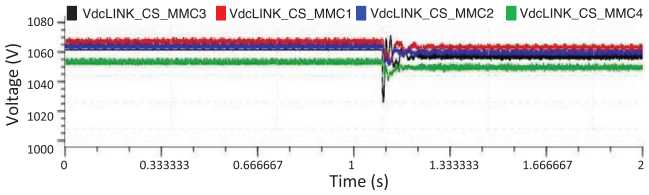

FIGURE 6 Voltages at DC side of converters during deblocking event.

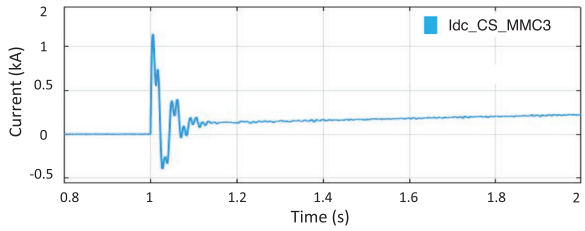

FIGURE 7 Current at PCC during deblocking of MMC3 converter.

CCSC loop once optimal set points for the ADC are determined. Finally, the optimal values obtained after key parameter adjustments of the ADC and enhanced CCSC are verified to ensure that all key parameters are configured optimally, thereby concluding the process.

6 | FINE TUNING OF KEY PARAMETERS

This study investigates a four-terminal MTDC network (Figure 1) without DC circuit breakers. Figure 5 represents the initial voltages, currents at DC side of converter for a four terminal MTDC network. During a severe DC fault (for instance, DC short circuit) near MMC3, the switch on the DC side is instantaneously opened to isolate the fault, effectively blocking MMC3. Upon fault resolution, MMC3 is deblocked.

Figure 6 provides an overview of the effects of deblocking Converter MMC3 at all DC terminals (MMC1-MMC4) when no active damping controller is employed. At the moment of deblocking, noticeable voltage dips are observed near the DC side of the converters. Likewise, Figure 7 illustrates the current at the PCC during the deblocking of the converter, near MMC3. During this process, a peak overshoot of 1.1431 kA is observed, with a settling time of 0.15842 s.

TABLE 2 Parametric sensitivity analysis DC-voltage regulation method (a) low pass filter (b) PI control coefficients.

Gain (G)	Time constant (TC)	Peak overshoot value (kA)	Settling time (s)
0.1	1	0.508874	0.10448
0.4	0.7	0.462252	0.1164
0.5	0.6	0.627815	0.1277
0.9	0.2	0.429801	0.11522
1	0.1	0.561325	0.17504
1.1	0.09	0.613680	0.14924
1.4	0.06	0.605960	0.12354
2	0.02	0.591391	0.14258
2.5	0.01	0.752649	0.16358
3	0.001	0.649669	0.17627

(a)

Proportional gain (K_P)	Integral time constant (ITC)	Peak overshoot value (kA)	Settling time (s)
0.2	0.9	0.613245	0.11798
0.4	0.7	0.435463	0.10706
0.6	0.5	0.685091	0.12928
1	0.1	0.610438	0.1181
1.5	0.05	0.550054	0.1469
2	0.02	0.538552	0.17306
2.5	0.01	0.674545	0.1166
3	0.005	0.585054	0.126272
5	0.003	0.572539	0.11966
8	0.001	0.60384	0.12452

(b)

To facilitate improved postfault recovery, a DC voltage regulation method is adopted as an active damping controller. Parametric sensitivity analysis is conducted on the crucial parameters of the DC voltage regulation method, specifically the low pass filter (LPF), where stability relies on the relationship between the gain (G) and the time constant (TC). Experimentation is employed to fine-tune the values of G and TC. Table 2a and Figure 8a demonstrate the outcomes for various G and TC values at the moment the MMC3 converter is deblocked, as shown in Figure 7, subsequent to recovery from a severe DC fault. The results indicate the optimal values of a gain at 0.9 and time constant at 0.2. Furthermore, variations in G and TC lead to an increase in peak overshoot value and settling time.

Following the LP filter is the dead-band controller, where values are chosen to prevent oscillations of the dead band controller output around the setpoint, ensuring the controller remains responsive to changes in the error signal. In this case study, the DC reference and measured DC voltage are considered in per unit. Consequently, the error becomes zero when the measured DC voltage equals the DC reference. For the study, high level and low level thresholds are maintained at 1.05 and 0.95, respectively, while the slope is set at 1. Optimizing the

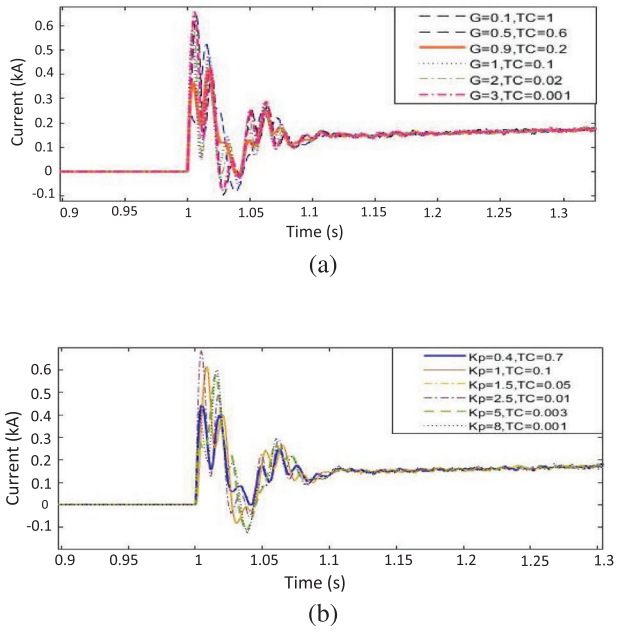

FIGURE 8 Parametric sensitivity analysis DC-voltage regulation method (a) low pass filter (b) PI control coefficients.

PI controller K_P (proportional gain) and integral time constant (ITC) is critical to determine the controller's sensitivity to the error signal and eliminate steady state error. Different values of K_P and ITC are examined to achieve the desired response for the DC voltage to closely track the DC reference. Table 2b and Figure 8b present various combinations of K_P and ITC, with the optimal values determined as 0.4 and 0.7, resulting in a notable reduction in overshoot time and settling time at the PCC point when the MMC3 converter is deblocked. Additionally, a rate limiter is incorporated to prevent the PI controller from making rapid and significant output changes, which could potentially lead to instability. The rate limiter's limits are set to control the rate of change of the PI controller's output. The optimal values derived from the parametric sensitivity analysis for the DC voltage regulation method are utilized and introduced as input to the inner control loop. As detailed in above section, the modified D-Q CCSC involves the tuning of the band-pass filter and PI controller to minimize the influence of zero-sequence non-DC elements. The frequency of the bandpass filter should be carefully selected to permit the desired frequency components to pass through while suppressing frequencies beyond this designated range.

Table 3 presents the results of the frequency domain analysis, aiding in the selection of the band-pass filter's cutoff frequency based on the gain margin (GM) and phase margin (PM). For a cutoff frequency of 300 Hz, a GM of 0.42 and a PM of 47.36 degrees suggest that the system remains stable, offering some flexibility for adjustments in gain. However, the PM is a crucial indicator for stability. A PM within the range of 45 to 90 degrees is generally considered favourable for stability. For a 300 Hz cutoff frequency, it indicates a better filter response. With a cutoff frequency of 350 Hz, a GM of 8.23 signifies a comfortable gain margin, indicating favourable stability. A PM of 5.83 degrees further indicates the system is much closer to instability compared to 300 Hz. A small phase margin translates to a higher risk of oscillations and potential signal distortion within the filter's passband. However, at frequencies of 400, 500, and 600 Hz, GM are still very low, indicating that the system is susceptible to gain-related issues like unwanted amplification of noise. Nevertheless, the negative phase margins of −11.43, −161.06, and −116.79 degrees raise concerns. A negative phase margin of such magnitude implies that the system is likely to be unstable or highly underdamped, potentially leading to oscillations or poor transient response.

TABLE 3 Frequency domain analysis to select cut-off frequency of BPF

Cut-off frequency	Gain margin	Phase margin
300 Hz	0.42	47.36
350 Hz	8.23	5.85
400 Hz	2.80	−11.43
500 Hz	3.21	−161.06
600 Hz	0.90	−116.79

TABLE 4 Tunning of PI control coefficients of D-Q CCSC

Proportional gain (K_P^{CCSC})	Integral time constant (ITC^{CCSC})	Peak overshoot value (kA)	Settling time (s)
0.1	1	0.640762	0.1277
0.5	0.6	0.599984	0.147001
0.7	0.4	0.53367	0.11762
1	0.1	0.499549	0.14096
1.1	0.09	0.411469	0.11174
1.5	0.05	0.523293	0.1457
2	0.02	0.606246	0.1481
2.5	0.01	0.468817	0.16982
3	0.005	0.484841	0.15914

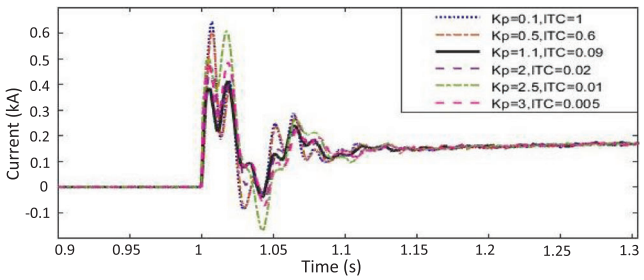

FIGURE 9 Parametric sensitivity analysis for PI control coefficients of enhanced D-Q CCSC.

Moreover, the PI controller is meticulously adjusted while examining the response with varying values, as illustrated in Table 4 and Figure 9. An increase in K_P^{CCSC} from 0.1 to 1.1 correlates with decrease in the peak overshoot value. This reduction aligns with expectations, as higher K_P^{CCSC} values correspond to

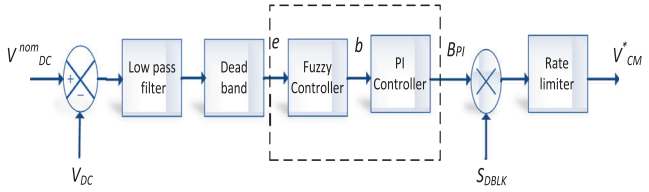

FIGURE 10 Enhanced DC voltage regulation method.

less overshoot, given the amplified control action of the proportional gain. Significantly, the settling time diminishes when ITC^{CCSC} is reduced from 1 to 0.09. This shift occurs due to the smaller ITC^{CCSC} value, enabling the integral action to promptly accumulate and rectify errors. However, further escalation of K_P^{CCSC} and ITC^{CCSC} values would lead to increased peak overshoot and settling time. Consequently, the controller with $K_P^{CCSC} = 1.1$ and $ITC^{CCSC}C = 0.09$ strikes a balance, yielding relatively low overshoot (0.411469 kA) and a rapid settling time (0.11174 s). With the finely tuned parameters of the damping controller and CCSC, the reduction in overshoot and settling time amounts to 64.00% and 29.47%, respectively, compared to the MTDC network without the use of an active damping controller, as depicted in Figure 9 compared to Figure 7.

7 | PROPOSED CONTROLLER FOR DAMPING OSCILLATIONS

This study proposes a novel control approach for HVDC networks: a coordinated FLC and PI controller for improved damping performance. The FLC leverages its ability to handle non-linearities, such as changing power flow patterns, which can significantly impact oscillation behaviour. This allows the FLC to adapt the control strategy in real-time. The PI controller provides a well-established framework for achieving good overall system performance. By combining these strengths, the coordinated FLC-PI approach has the potential to lead to faster settling times and reduced overshoot compared to traditional methods. The active damping controller (ADC) circuit examined here is a DC voltage regulation method consisting of a PI controller and a fuzzy controller, as depicted in Figure 10. The fuzzy controller acts as a pre-processing stage for the PI controller, enabling it to handle non-linearities (such as saturation in converter outputs) and effectively transforming the input for the PI controller. Thus, a coordinated approach, integrating fuzzy control alongside traditional PI controllers, offers a practical way to leverage the advantages of fuzzy logic without complete replacement [22].

Further, designing a steps of a fuzzy controller is a crucial step in this approach. A fuzzy logic controller requires appropriate ranges for input and output values, membership functions, a fuzzification method, a set of if-then rules, and a defuzzification method. The fuzzy logic controller is shown in Figure 11. The inputs to the fuzzy controller are derived from error signal (e) and the rate of change of error (de). A fuzzy logic controller is composed of three fundamental stages [21, 23].

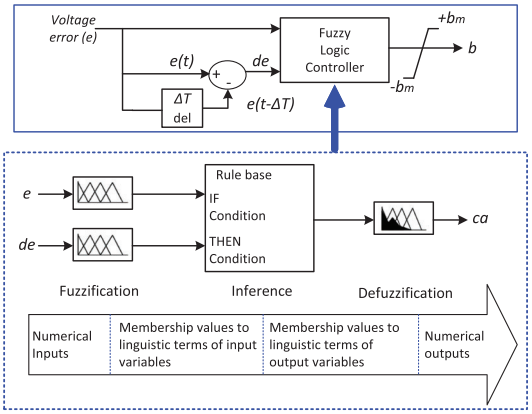

FIGURE 11 Fuzzy logic controller with structure of a fuzzy system with numerical inputs '*e*', '*de*' and numerical outputs '*ca*'.

- **Fuzzification**: This initial stage converts crisp numerical input values (e.g. error signal (e) and rate of change of error (de)) into fuzzy membership values. Each crisp input is assigned a degree of membership to the fuzzy sets based on the chosen membership function.
- **Interface mechanism**: This stage acts as the decision-making core of the FLC. Fuzzy inputs are mapped into fuzzy decisions using a set of linguistic if-then rules stored in the fuzzy rule base. These rules typically employ logical operators like AND (min function) and OR (max function) to combine fuzzy inputs (antecedents) and generate a fuzzy output (consequent). The antecedent is a weighted fuzzy input with a single number, while the consequent is a fuzzy set shaped by a membership function. Aggregation methods (e.g. maximum, probabilistic OR) are then used to combine the outputs (consequents) of each rule into a single fuzzy set. Common inference mechanisms used to draw conclusions from fuzzy knowledge include the "Mamdani" and "Sugeno" models. The key difference lies in the output stage: the Mamdani model uses fuzzy output membership functions, while the Sugeno model employs a weighted average of the consequents, which are no longer fuzzy sets but often linear formulas for calculating the crisp output.
- **Defuzzification**: The final stage transforms the aggregated fuzzy set from the rule base into a single crisp output value (ca) that can be used as a control signal for the system. Various defuzzification methods exist, such as centroid method (centre of gravity (CoG)), bisector, and largest of maximum [24]. The specific method chosen can influence the control behaviour of the FLC. The fuzzy interface process is illustrated in Figure 11.

A crucial aspect of this FLC design is balancing complexity and control effectiveness for damping DC-side oscillations in HVDC networks. This study uses five linguistic values for both the error (e) and the rate of change of error (de): "negative high (nh)," "negative (n)," "zero (z)," "positive (p)," and "positive high (ph)." This choice offers several advantages:

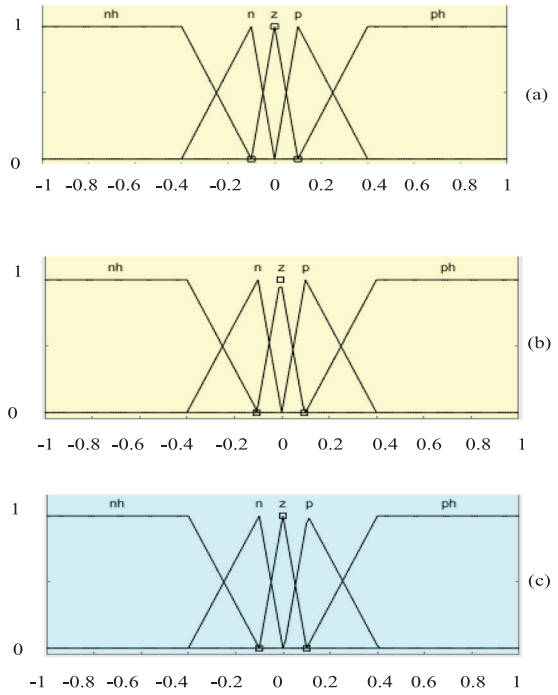

FIGURE 12 Membership functions of (a) input variable (error '*e*'), (b) input variable (difference in error '*de*'), (c) output variable (control action '*ca*').

- **Reduced rule complexity**: Using five values minimizes the number of fuzzy sets and rules needed for effective control, balancing granularity and computational efficiency. This prevents overfitting and keeps the rule base manageable.
- **Effective control for oscillation damping**:
  1. Magnitude of error: The five values represent different error magnitudes in DC voltage, allowing the FLC to tailor its response based on the severity of oscillations.
  2. Adapting to error dynamics: Including the rate of change of error (*de*) helps the FLC dynamically adjust its response. For example, a large negative error with a rapidly decreasing rate may need less aggressive correction, whereas a sustained error with an increasing rate requires stronger corrective action. By capturing both the magnitude and rate of change of the error signal, these five linguistic values enable the FLC to make precise adjustments to the DC voltage.

The design employs triangular (*trimf*) and trapezoidal (*trapmf*) membership functions (MFs) to represent linguistic values within the range of [−1, 1]. These MFs are simple, computationally efficient, and offer smooth transitions, ensuring a stable control system. The width and slopes of these MFs influence the overlap and smoothness of the transition between fuzzified sets, as illustrated in Figure 12.

Once fuzzification is done, it translates precise data into fuzzy sets, enabling the system to reason with linguistic rules based on these sets. The fuzzy controller utilizes a set of if-then rules to determine the appropriate control action for regulating DC voltage. These rules consider both the error (*e*) and the rate of change of error (*de*) as illustrated by Table 5 which represent FLC decision making strategy.

TABLE 5 Fuzzy rules.

e		*nh*	*n*	*z*	*p*	*ph*
de	*nh*	*nh*	*nh*	*nh*	*n*	*z*
	n	*nh*	*nh*	*n*	*z*	*p*
	z	*nh*	*n*	*z*	*p*	*ph*
	p	*n*	*z*	*p*	*ph*	*ph*
	ph	*z*	*p*	*ph*	*ph*	*ph*

Five linguistic values for the output (control action) are considered: "negative high (*nh*)," "negative (*n*)," "zero (*z*)," "positive (*p*)," and "positive high (*ph*)." This choice offers a range of control actions that translate into adjustments to the reference for active power injection. These adjustments, provided to the PI controller, ultimately influence the converter control system to regulate the DC voltage and effectively dampen oscillations. Each rule maps a combination of error and rate of change values (e.g. "large negative error, *nh*" and "rapidly decreasing, *nh*") to a specific control action ("decrease output significantly, *nh*"). These values allow the FLC to make dynamic adjustments to the desired active power injection based on the system's behaviour.

For example in Table 5, If the error is significantly negative($e = nh$) (large voltage drop), the FLC increases active power injection (decrease control action (output)) to counter the voltage drop. Further, a rapidly decreasing rate of change ($de = nh$) alongside a significant negative error ($e = nh$) indicates a quickly worsening voltage drop. This is reflected in rule: "If *e* is '*nh*' and *de* is '*nh*,' then control action is '*nh*'"). Further, if the error is significantly negative ($e = nh$) but the rate of change is positive ($de = p$), it suggests the voltage is decreasing but starting to recover. A fuzzy rule like: If *e* is '*nh*' and *de* is '*p*', then control action is '*n*') reflects such case. For smaller errors ($e = n, p$), the FLC might adjust active power more moderately based on the error severity and rate of change (e.g. If *e* is '*z*' and *de* is '*p*', then control action is '*p*'). When the error is zero ($e = z$) (desired voltage is achieved), the FLC aims to maintain the voltage by keeping the control action around zero (e.g. If *e* is '*z*' and *de* is '*z*', then control action is '*z*').

The max–min inference operator, a popular method in fuzzy control systems, is employed to evaluate the if-then rules in this study. The inference engine incorporated the Mamdani fuzzy model. The well-known COG method is a popular defuzzification choice due to its computational efficiency and intuitive output generation [19, 24]. This allows for the conversion of fuzzy outputs into crisp values for control decisions.

The PI controller takes the crisp control signal from the defuzzifier as its input. It combines the signal (*b*) with its proportional gain (K_p) and time constant (T_i) to adjust the final control output (B_{PI}). The K_p and T_i values are considered 0.4 and 0.7, which were obtained after fine-tuning the PI controller using a trial and error approach as discussed in Section 6.

TABLE 6 Outcomes of different controllers used in the study.

Controller	Peak-overshoot value (kA)	Settling time (s)
PI	0.411468	0.11174
Fuzzy	0.429850	0.12421
Fuzzy +PI	0.330971	0.10016

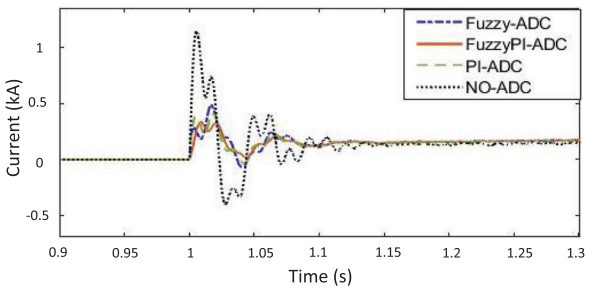

FIGURE 13 Performance of ADC using fuzzy controller, PI controller, enhanced controller and without ADC.

A user defined module for the FLC has been created using component builder (c-builder) facility available in RSCAD simulation tool and PI controller is added to it. The controller works as a coordinated fuzzy & PI controller. The proposed ADC controller is tested using four-terminal terminal MMC-based MTDC network as shown in Figure 1, where proposed ADC shown in Figure 10 is used in outer loop for damping the oscillations at DC side of converter during post fault recovery. The current at the PCC during the deblocking of the converter is observed during deblocking of the converter (MMC3) after subsequent recovery from DC fault.

Table 6 and Figure 13 illustrate the outcomes of the advanced controller used in the ADC, comparing the performance of ADC with fuzzy controller, PI controller, coordinated fuzzy PI controller, and without ADC (baseline scenario when no ADC is used) during the deblocking of the MMC3 converter following recovery from a severe DC fault. As discussed in the Section 6, when no ADC is used, the current at PCC during the deblocking of the converter is depicted by the black dotted line in Figure 13. During this process, a peak overshoot of 1.1431 kA is observed, with a settling time of 0.15842 s. With a fine-tuned PI controller used in ADC, a reduction in overshoot and settling time by 64.00% and 29.47%, respectively, is observed. When only a fuzzy controller is used in ADC, a reduction in overshoot by 62.40% and decrease in settling time by 21.57% are noted. For better post fault recovery after severe DC fault, the coordinated fuzzy PI controller achieves the best performance leading to reduction in overshoot by 71.05% and settling time by 36.78% compared to when no ADC is used. Further, the enhanced controller achieved a significant 19.56% reduction in overshoot and a 10.36% reduction in settling time compared to the fine-tuned PI controller used in the DC -side voltage regulator approach [7].

The investigation is extended to the MMC4 converter using the enhanced ADC, assuming the same fault conditions as

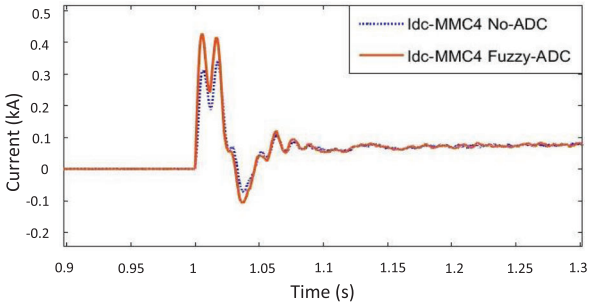

FIGURE 14 Current at PCC during deblocking using ADC fuzzy control for MMC4 converter.

TABLE 7 Performance evaluation of enhanced controller.

Method	Reference	Reduction in overshoot (%)	Reduction in settling time (%)
Enhanced fuzzy + PI controller	—	19.56	10.36
D-Q CCSC with	[10]	2.59	3.57
Modulated signal CCSC-MPC	[11]	—	13.6
Modified D-Q CCSC	[26]	7	12

previously discussed for the MMC3 converter terminal. The impact of a fault near the MMC4 converter terminal is analyzed as shown in Figure 14. With fuzzy-ADC, the peak overshoot is 0.31953 kA, and the settling time is 0.1628 s. In contrast, without ADC, the overshoot current is 0.42823 kA, and the settling time is 0.23588 s. The percentage improvement in peak overshoot is 25.38%, and the improvement in settling time is 30.98% when using fuzzy-ADC compared to no ADC for the MMC4 converter.

The enhanced ADC is compared to some key existing approaches from the literature review, as enhanced fuzzy-PI controller achieves a significant 19.56% reduction in overshoot, demonstrating exceptional transient response improvement and provides better damping of oscillations. This translates to faster settling time (10.36%), indicating a quicker reduction in steady-state error. The comparison with other key approaches is shown in Table 7 which shows the effectiveness of enhanced approach when compared with key performance indices such as overshoot time and settling time.

So, the coordinated fuzzy-PI controller emerges as the most effective strategy for mitigating current fluctuations during the deblocking process of the converter (MMC3). This success hinges on its ability to leverage the strengths of both approaches: fuzzy logic component provides adaptability by handling the non-linearities and uncertainties inherent in the HVDC networks. This allows the controller to react swiftly to the initial change in operating point, minimizing overshoot and PI control for precision as the controller component ensures precise adjustments and effective damping of system

oscillations. This collaboration leads to a faster settling time and overall better performance.

However, it's crucial to remember that the effectiveness of the coordinated fuzzy-PI controller is highly dependent on the design of the fuzzy logic component. The choice of linguistic values, membership functions, and rule base all significantly influence the controller's ability to interpret system states and generate appropriate control actions. Careful design and optimization of these fuzzy logic elements are essential to unlock the full potential of this powerful control strategy.

8 | CONCLUSION

This study overviews a thorough examination and a new control functionality for oscillation damping of an MTDC interconnected offshore-onshore system. The research is done by utilizing EMT-based simulations. It addresses research gaps concerning sub-synchronous oscillation damping on the DC side of HVDC networks. Specifically, it delves into a DC-voltage regulation method paired with a modified CCSC to enhance post-fault recovery of the converter. The study conducts meticulous parametric sensitivity analysis to evaluate system performance, resulting in a notable 34.46% reduction in overshoot and a 12.50% improvement in settling time compared to the initial controller parameterization. These findings contribute to the refinement of post-fault recovery mechanisms, bolstering the resilience of complex offshore-onshore HVDC networks.

Furthermore, the study extends its scope by introducing a coordinated fuzzy-PI controller to enhance controller performance. This approach offers an enhanced and adaptable strategy compared to traditional PI controllers in DC voltage regulation. The coordinated fuzzy-PI controller demonstrates significant improvements in post-fault recovery, evidenced by a 19.56% reduction in current overshoot. This enhancement translates to exceptional transient response improvement and better oscillation damping. Further, resulting in a 10.36% faster settling time indicating a quicker reduction in steady-state error. Overall, this research underscores the potential of coordinated fuzzy-PI control in enhancing the dynamic performance and fault tolerance of MMC-based MTDC networks, thus contributing to the resilience of AC/DC networks.

AUTHOR CONTRIBUTIONS

Monika Sharma: Writing—original draft; writing—review and editing. **José L. Rueda Torres**: Writing—review and editing.

ACKNOWLEDGEMENTS

HVDC-WISE is supported by the European Union's Horizon Europe programme under agreement 101075424. UK Research and Innovation (UKRI) funding for HVDC-WISE is provided under the UK government's Horizon Europe funding guarantee [grant numbers 10041877 and 10051113]. Views and opinions expressed are however those of the author(s) only and do not necessarily reflect those of the European Union or European Climate, Infrastructure and Environment Executive Agency. Neither the European Union nor the granting authority can be held responsible for them.

CONFLICT OF INTEREST STATEMENT

The authors declare no conflicts of interest.

DATA AVAILABILITY STATEMENT

The data that support the findings of this study are available from the corresponding author upon reasonable request.

ORCID

Monika Sharma https://orcid.org/0000-0001-8996-2369

REFERENCES

1. Saeedifard, M., Graovac, M., Dias, R., Iravani, R.: DC power systems: challenges and opportunities. In: IEEE PES General Meeting, pp. 1–7. IEEE, Piscataway, NJ (2010)
2. Cole, S., Karoui, K., Vrana, T.K., Fosso, O.B., Curis, J., Denis, A.M., et al.: A European supergrid: present state and future challenges. In: Proceedings of the 17th Power Systems Computation Conference (PSCC), pp. 1–7. PSCC, Zürich (2011)
3. Yang, H., Dong, Y., Li, W., He, X.: Average-value model of modular multilevel converters considering capacitor voltage ripple. IEEE Trans. Power Delivery 32(2), 723–732 (2016)
4. Trinh, N.T., Zeller, M., Wuerflinger, K., Erlich, I.: Generic model of MMC-VSC-HVDC for interaction study with ac power system. IEEE Trans. Power Syst. 31(1), 27–34 (2015)
5. Padiyar, K.: HVDC Power Transmission Systems: Technology and System Interactions. New Age International, New Delhi (1990)
6. Enslin, J.H., Heskes, P.J.: Harmonic interaction between a large number of distributed power inverters and the distribution network. IEEE Trans. Power Electron. 19(6), 1586–1593 (2004)
7. Abedrabbo, M., Dejene, F.Z., Leterme, W., Van-Hertem, D.: HVDC grid post-DC fault recovery enhancement. IEEE Trans. Power Delivery 36(2), 1137–1148 (2020)
8. Basu, M., Mahindara, V.R., Kim, J., Nelms, R.M., Muljadi, E.: Comparison of active and reactive power oscillation damping with PV plants. IEEE Trans. Ind. Appl. 57(3), 2178–2186 (2021)
9. Me, S.P., Zabihi, S., Blaabjerg, F., Bahrani, B.: Adaptive virtual resistance for postfault oscillation damping in grid-forming inverters. IEEE Trans. Power Electron. 37(4), 3813–3824 (2021)
10. Liu, Y., Raza, A., Rouzbehi, K., Li, B., Xu, D., Williams, B.W.: Dynamic resonance analysis and oscillation damping of multiterminal DC grids. IEEE Access 5, 16974–16984 (2017)
11. Virulkar, V., Gotmare, G.: Sub-synchronous resonance in series compensated wind farm: a review. Renewable Sustainable Energy Rev. 55, 1010–1029 (2017)
12. Kumar, N., Singh, B., Panigrahi, B.K.: Voltage sensorless based model predictive control with battery management system: for solar PV powered on-board EV charging. IEEE Trans. Transp. Electrif. (2022)
13. D'Arco, S., Suul, J.A., Molinas, M.: Implementation and analysis of a control scheme for damping of oscillations in VSC-based HVDC grids. In: 2014 16th International Power Electronics and Motion Control Conference and Exposition, pp. 586–593. IEEE, Piscataway, NJ (2014)
14. Li, C., Li, Y., Cao, Y., Zhu, H., Rehtanz, C., Häger, U.: Virtual synchronous generator control for damping DC-side resonance of VSC-MTDC system. IEEE J. Emerg. Sel. Top. Power Electron. 6(3), 1054–1064 (2018)
15. Pinares, G., Bongiorno, M.: Modeling and analysis of VSC-based HVDC systems for DC network stability studies. IEEE Trans. Power Delivery 31(2), 848–856 (2015)
16. Van.Hertem, D., Ghandhari, M., Delimar, M.: Technical limitations towards a supergrid–a European prospective. In: 2010 IEEE International Energy Conference, pp. 302–309. IEEE, Piscataway, NJ (2010)

17. Deng, J., Cheng, F., Yao, L., Xu, J., Mao, B., Li, X., et al.: A review of system topologies, key operation and control technologies for offshore wind power transmission based on HVDC. IET Gener. Transm. Distrib. 17(15), 3345–3363 (2023)
18. Rosa, A., Morais, L., Fortes, G., Júnior, S.S.: Practical considerations of nonlinear control techniques applied to static power converters: a survey and comparative study. Int. J. Electr. Power Energy Syst. 127, 106545 (2021)
19. Daneshpooy, A., Gole, A., Chapman, D., Davies, J.: Fuzzy logic control for HVDC transmission. IEEE Trans. Power Delivery 12(4), 1690–1697 (1997)
20. Muyeen, S., Hasanien, H.M.: Operation and control of HVDC stations using continuous mixed p-norm-based adaptive fuzzy technique. IET Gener. Transm. Distrib. 11(9), 2275–2282 (2017)
21. kumari Kovvuru, A., Dewangan, P.: Design of fuzzy-PID controller using optimization technique based reduced order modelling. In: 5th International Conference on Energy, Power and Environment: Towards Flexible Green Energy Technologies (ICEPE), pp. 1–5. IEEE, Piscataway, NJ (2023)
22. Mohammadzadeh, A., Sabzalian, M.H., Zhang, C., Castillo, O., Sakthivel, R., El-Sousy, F.F.: Modern Adaptive Fuzzy Control Systems. Springer, Cham (2023)
23. Lee, C.C.: Fuzzy logic in control systems: fuzzy logic controller. I. IEEE Trans. Syst. Man Cybern. 20(2), 404–418 (1990)
24. Nguyen, A.T., Taniguchi, T., Eciolaza, L., Campos, V., Palhares, R., Sugeno, M.: Fuzzy control systems: past, present and future. IEEE Comput. Intell. Mag. 14(1), 56–68 (2019)
25. Shetgaonkar, A., Karmokar, T., Popov, M., Lekić, A.: Enhanced real-time multi-terminal HVDC power system benchmark models with performance evaluation strategies. CIGRE Sci. Eng. 62, 1–29 (2024)
26. Freytes, J., Bergna, G., Suul, J.A., D'Arco, S., Gruson, F., Colas, F., et al.: Improving small-signal stability of an MMC with CCSC by control of the internally stored energy. IEEE Trans. Power Delivery 33(1), 429–439 (2017)

How to cite this article: Sharma, M., Torres, J.L.R.: Enhanced post-fault recovery in MTDC networks using active damping approach. IET Gener. Transm. Distrib. 19, e13321 (2025). https://doi.org/10.1049/gtd2.13321